J. Phys. B: At. Mol. Opt. Phys. **31** (1998) 3949–3964. Printed in the UK PII: S0953-4075(98)90334-0

Low-energy electron scattering from xenon

J C Gibson†, D R Lun†, L J Allen‡, R P McEachran†, L A Parcell§ and S J Buckman†

† Atomic and Molecular Physics Laboratories, Research School of Physical Sciences and Engineering, Australian National University, Canberra, ACT 0200, Australia

‡ School of Physics, University of Melbourne, Parkville, 3052, VIC, Australia

§ MPCE, Macquarie University, North Ryde, NSW, Australia

Received 6 January 1998

Abstract. A detailed experimental and theoretical study of elastic electron–xenon scattering has been carried out for incident electron energies between 0.67 and 50 eV. The experimental measurements have been conducted using a crossed-beam apparatus and the relative flow technique, while the theoretical calculations are a fully relativistic treatment which also includes the effects of polarization and dynamic distortion. The experimental results (absolute differential cross sections) have been analysed with a relativistic version of a phase-shift analysis program in an effort to extract the low-order phase shifts, including the two spin–orbit components of the low-energy p-wave phase shift, and to derive the total elastic and elastic momentum transfer cross sections. Extensive comparisons between the present measurements and calculations and previous experiment and theory are provided.

1. Introduction

It has been well established that relativistic interactions can be very important in the scattering of electrons from heavy atomic targets, even when the impact energy is very low (a few eV). Indeed these effects can be so large that they even manifest themselves in the integral cross sections for elastic scattering from systems such as krypton and xenon where, for example, recent relativistic scattering calculations show significant differences in the position of the Ramsauer–Townsend (R–T) minima from that observed in similar calculations performed in a non-relativistic framework (McEachran and Stauffer 1987).

Low-energy electron scattering from xenon has been the subject of much experimental and theoretical investigation in recent years. Whilst it is not appropriate to detail all of this work here, it is worth noting that with which we shall compare the present measurements, in particular those measurements at energies below 5 eV which is our main area of interest. At energies below 2 eV there is an extensive set of measurements of elastic differential cross sections (DCS) by Weyhreter *et al* (1988), although the angular range of these measurements is limited (20–100°). At higher energies Klewer *et al* (1980) measured elastic DCS between 2 and 300 eV, Nishimura *et al* (1987) from 5 to 200 eV and Register *et al* (1986) for incident energies between 1 and 100 eV. McEachran and Stauffer (1984, 1987, 1988) have applied several versions of the polarized orbital method to e^-–Xe scattering, including a model which involved the solution of the Dirac equation to account for relativistic interactions. Johnson and Guet (1994) have calculated low-energy elastic scattering phase shifts using relativistic many-body perturbation theory. Gianturco and Rodriguez-Ruiz (1994) have applied density functional theory to calculate differential and total scattering cross sections,

0953-4075/98/173949+16$19.50

and Yuan (1995) has used Dirac–Fock wavefunctions for a calculation of elastic DCS from 0.5 to 10 eV.

To date almost all direct experimental investigations of relativistic effects, such as the spin–orbit interaction, have been made with either spin-polarized incident electron beams or by measuring the polarization of the scattered electrons, in order that the spin dependence of the scattering process can be readily studied. These experiments usually involved the measurement of the Sherman function, where the differences between the elastic DCS for spin-up and spin-down electrons is expressed as an asymmetry (Kessler 1985, 1991). In the present series of experiments and calculations, we have attempted to exploit the fact that for low-energy electron scattering from the heavy rare gas atoms in the region of the R–T minimum, the contribution to the elastic scattering cross section from the $l = 0$ partial wave is vanishingly small. As a result, detailed differential elastic scattering measurements in the energy region of the R–T minimum for Xe ($\sim$0.8 eV) should provide a sensitive probe of the higher-order phase shifts and, as the energy is still reasonably low, the p- and d-wave phase shifts in particular. Furthermore, relativistic elastic scattering calculations which have been carried out as part of this study, indicate that the two components of the p-wave phase shift ($p_{1/2,3/2}$) are both very small and significantly different (about a factor of 2) in magnitude in the R–T minimum region, whilst the two d-wave components ($d_{3/2,5/2}$) only differ by a few per cent. Thus, accurate DCS measurements over a fine angular and energy grid in the region of 1 eV, combined with a 'relativistic' formulation of a phase-shift analysis technique which allows for two spin–orbit components for the p-wave phase shift only, have the potential to provide experimental information on these spin-dependent phase shifts from an unpolarized electron scattering experiment. These can in turn be used to provide an estimate of the Sherman function for energies below 2 eV, where there are no previous experimental measurements. The results of this aspect of the work have been presented and described in a recent letter (Buckman *et al* 1997).

In this work we have measured absolute elastic DCS at 10 electron energies below the first inelastic threshold (8.32 eV) and at 10, 20, 25, 40 and 50 eV. At each energy we have also calculated the DCS using the relativistic, dynamic distortion approach and we have applied the relativistic, phase-shift analysis to extract the first few scattering phase shifts from the experimental data at all energies below the first inelastic threshold.

In the following section the experimental apparatus and techniques are briefly described, followed by a discussion of the theoretical calculations and the phase-shift analysis technique in section 3. We then present the results, comparing the present theory and experiment with previous work and provide a few concluding remarks.

2. Experimental apparatus and techniques

The present experimental apparatus has been described in substantial detail in a number of recent publications (see e.g. Gulley *et al* 1994) so we shall restrict ourselves in this section to the description of those matters which are central and particular to the present xenon measurements. The DCS are measured with a crossed-beam geometry, the atomic beam effusing from a capillary array of 1 mm active diameter consisting of 40 μm diameter, 1 mm long capillaries. The electron beam is produced by a combination of a thoriated tungsten filament, electrostatic electron optics and a hemispherical electrostatic monochromater. Scattered electrons are energy analysed and detected by a similar electrostatic analyser which can rotate about the atomic beam axis to enable access to scattering angles from -15° to 130°. The overall energy resolution of the apparatus for the present measurements is typically 60–80 meV. The absolute energy scale is determined by measurements of the

position of the resonance structure in elastic scattering from N_2, Xe and He. At low energies we calibrate against the position of the second quasivibrational resonance peak in elastic scattering from N_2 which, at a scattering angle of 60°, occurs at an energy of 2.198 eV (Rohr 1977). At higher energies, the incident energy is calibrated against the position of the Xe^- $5p^5\,{}^2P_{3/2}\,6s^2$ resonance in the elastic electron scattering channel at 7.90 eV (see e.g. Buckman and Clark 1994). Finally, for energies above 20 eV we use the He^- $1s2s^2\,{}^2S$ resonance at 19.367 eV as the energy calibration. In practice this crosscheck has proved useful as it has highlighted possible nonlinearities in the energy scale of as much as 200 meV between 2 and 20 eV, which depend to a large extent on the electron optical settings and the gas mixtures.

The measured angular distributions for elastic electron scattering from xenon are placed on an 'absolute' scale by the use of the relative flow technique in conjunction with the 'standard' elastic scattering cross sections for helium. In this case we have used the calculated cross sections of Nesbet (1979) at energies below the first inelastic threshold for helium (∼19.8 eV). At higher energies we have used the helium elastic scattering cross sections, previously measured in this laboratory by Brunger *et al* (1992), as the reference. The application of the relative flow technique in the present apparatus has been described in a number of recent papers (Buckman *et al* 1993, Gulley *et al* 1994) and we will not repeat that detail here. However, as in a number of previous applications in our laboratory (e.g. Alle *et al* 1992, Gulley *et al* 1994), the relative flow rates for Xe and He were determined from a separate series of experiments and a calibration function was established which could be used to convert the driving pressure ratio for the two gases, which is readily measured during the experimental data collection, to a ratio of flow rates for use in the relative-flow cross section calculation. We also note that both gases, Xe and He, were present in the apparatus at all times in an effort to reduce contact potential variations. This is achieved by having one gas flowing to the capillary array for the scattering measurements whilst the other gas enters the chamber through a capillary on the chamber periphery. The advantages of this approach have been discussed previously (Gulley *et al* 1993).

3. Theoretical calculations

The original polarized-orbital approximation (Temkin 1957, Temkin and Lamkin 1961) was developed in order to take into account the dominant long-range adiabatic interaction between the incident electron and the atom. This interaction usually has been described in terms of an adiabatic multipole polarization potential. Nonetheless, it was also recognized that, in electron scattering, the neglect of the effects of the motion of the incident electron would lead to an interaction that became increasingly too attractive as the incident energy increased.

LaBahn and Callaway (1966) and Callaway *et al* (1968) introduced a formalism whereby these dynamic effects could be incorporated into the polarized-orbital approximation. Unfortunately, however, their results were somewhat inconclusive since for helium they just used scaled hydrogenic polarization and distortion potentials. Since then these dynamic distortion effects have been included within the general framework of the polarized-orbital method and applied to the elastic scattering of electrons from helium (McEachran and Stauffer 1990) and from neon, argon and krypton (Mimnagh *et al* 1993). In these calculations, which were carried out within a non-relativistic framework, both the polarization and distortion potentials included many multipoles, including the monopole terms. For helium, argon and krypton these calculations, including multipole polarization and dynamic distortion effects, gave improved agreement with experiment, particularly at

the lowest energies, vis-à-vis the previous adiabatic exchange results which included only the dipole polarization potential (McEachran and Stauffer 1983a, b, 1984).

We have also shown, within the adiabatic exchange approximation, that the low-energy total and momentum transfer cross sections for krypton (McEachran and Stauffer 1988) and xenon (McEachran and Stauffer 1987) were in much better agreement with experiment, particularly in the vicinity of the R–T minimum, if the phase shifts were determined from the solution of the relativistic Dirac scattering equations rather than from the equivalent non-relativistic Schrödinger equation. More recently, we have shown (McEachran and Stauffer 1997) that the inclusion of multipole polarization and dynamic distortion effects in the determination of the phases within this relativistic formalism gave excellent agreement for argon when compared with the experimental value for the scattering length (Petrovic *et al* 1995) as well as with the differential cross section between 1 and 10 eV (Gibson *et al* 1996).

In this paper, we employ polarization and dynamic distortion potentials to determine the relativistic phase shifts for xenon from the solution of the Dirac scattering equations. For a discussion of the asymptotic form of these potentials and the details of the equations involved in the determination of these relativistic phase shifts, the reader is referred to McEachran and Stauffer (1997).

Once the phase shifts have been determined, then the elastic differential cross section can be found from the expression

$$\sigma(\theta) = |f(\theta)|^2 + |g(\theta)|^2 \tag{1}$$

where

$$f(\theta) = \frac{1}{k}\sum_{l=0}^{\infty} f_l = \frac{1}{k}\sum_{l=0}^{\infty}\{(l+1)T_l^+(k) + lT_l^-(k)\}P_l(\cos\theta) \tag{2}$$

and

$$g(\theta) = \frac{1}{k}\sum_{l=0}^{\infty} g_l = \frac{1}{k}\sum_{l=0}^{\infty}\{(T_l^-(k) - T_l^+(k)\}P_l^1(\cos\theta) \tag{3}$$

are the direct and spin-flip scattering amplitudes respectively. The T-matrix elements, $T_l^{\pm}(k)$, are given in terms of the spin-up (δ_l^+) and spin-down (δ_l^-) phase shifts by

$$T_l^{\pm}(k) = \exp(\mathrm{i}\delta_l^{\pm}(k))\sin(\delta_l^{\pm}(k)) \tag{4}$$

and $P_l(\cos\theta)$ and $P_l^1(\cos\theta)$ are the Legendre and associated Legendre polynomials respectively. The total elastic cross section and the elastic momentum transfer cross section can then be expressed in terms of the phase shifts as

$$\sigma_{\mathrm{tot}}^{\mathrm{el}}(k^2) = \frac{4\pi}{k^2}\sum_{l=0}^{\infty}\{(l+1)\sin^2(\delta_l^+(k)) + l\sin^2(\delta_l^-(k))\} \tag{5}$$

and

$$\sigma_{\mathrm{mom}}^{\mathrm{el}}(k^2) = \frac{4\pi}{k^2}\sum_{l=0}^{\infty}\left\{\frac{(l+1)(l+2)}{2l+3}\sin^2(\delta_l^+(k) - \delta_{l+1}^+(k)) + \frac{l(l+1)}{2l+1}\sin^2(\delta_l^-(k) - \delta_{l+1}^-(k)) + \frac{(l+1)}{(2l+1)(2l+3)}\sin^2(\delta_l^+(k) - \delta_{l+1}^-(k))\right\}. \tag{6}$$

In these calculations the relativistic ground-state wavefunction of xenon was determined using the Dirac–Fock computer code of Grant *et al* (1980). This wavefunction was then

used to determine the static potential as well as in the evaluation of the exchange kernels. The polarization and distortion potentials, on the other hand, were determined from the first-order correction to the non-relativistic Hartree–Fock wavefunction for xenon. In these potentials all multipole components up to and including those which vanish at infinity as r^{-8} were included. The advantages of the inclusion of both distortion and relativistic effects, as in this calculation, have been demonstrated in a recent publication on argon (McEachran and Stauffer 1997).

4. Phase-shift analysis technique

There are a number of different ways to parametrize the T-matrix elements given above. Rational function forms, which are suitable for scattering problems involving a large number of partial waves, have been used by Allen (1986). In cases such as the present, where only the first few partial waves are important, we parametrize the phase shifts up to $l_{\max}$, where $l_{\max}$ varies between 2 and 4 depending on the incident energy, and calculate the higher-order phase shifts using the formula of Ali and Fraser (1977). Also for scattering at energies below 5 eV, the present scattering calculations, which were outlined above, indicate that the splitting of the two relativistic components of the phase shifts are only significant for the p-wave. As a result, in all cases except for the p-wave, δ_l^+ and δ_l^- are taken to be equal. Thus, the fitting process involves the use of between four and six adjustable parameters which are then determined by minimizing the function

$$\chi^2 = \sum_{i=1}^{M} \frac{[\sigma_i - \sigma(\theta_i)]^2}{(\Delta\sigma_i)^2} \tag{7}$$

where σ_i is the measured value of the DCS at the angle θ_i, with a statistical uncertainty $\Delta\sigma_i$, $\sigma(\theta_i)$ is the fitted value of the cross section at the angle θ_i, and M is the number of data points.

We have noticed that a twofold ambiguity to the solution exists in this fitting model. The differential cross sections are invariant to the transformation

$$\tilde{\delta}_l^{\pm} = \arctan \frac{(l+1)\sin(2\delta_l^+) + l\sin(2\delta_l^-)}{(l+1)\cos(2\delta_l^+) + l\cos(2\delta_l^-)} - \delta_l^{\pm} \tag{8}$$

on the p-wave phase shifts (i.e. $l = 1$). This can be readily seen by noting that, under this transformation, $f_1(\theta)$ and $|g_1|$ (and so $|g|$) are unchanged. If $\delta^{\pm}$ are both small, equation (8) becomes

$$\begin{aligned} \tilde{\delta}^{\pm} &\approx \frac{4\delta^+ + 2\delta^-}{3} - \delta^{\pm} \\ &= \delta^{\mp} + \frac{(\delta^+ - \delta^-)}{3}. \end{aligned} \tag{9}$$

Further, if $(\delta^+ - \delta^-)/3$ is small compared with $\delta^{\pm}$, which is true for $E \geqslant 5$ eV, then $\tilde{\delta}^{\pm} \approx \delta^M$ and the Sherman function for the two solutions will have opposite sign. Thus, it is not difficult to use theory or experiment to choose the physical solution and, as the Sherman functions change smoothly with energy, the correct solution can be determined from a measurement at a nearby energy, allowing this technique to be used in energy regions where there are presently no experimental Sherman function data for xenon. The accuracy of the fitting technique and its usefulness in deriving Sherman functions, have been discussed by Buckman *et al* (1997) and we shall not repeat that discussion here. However, the conclusion that arose from that work was that the Sherman functions derived from fitting

the present experimental DCS should be reliable up to an energy of about 3 eV whilst above this energy, the ability to extract relativistic information from such an unpolarized scattering experiment seems limited. However, the non-relativistic phase-shift analysis technique has still been pursued at these, and higher energies up to the first inelastic threshold, to enable the derivation of integral elastic and elastic momentum transfer cross sections from the measured DCS data, and to provide phase shifts for direct comparison with theory.

5. Results and discussion

5.1. Differential scattering cross sections

The absolute elastic differential cross sections obtained in this work are given in table 1 while comparisons with other recent low-energy experiment and theory, including the present calculation, are presented graphically in figures 1 and 2. The tabulated values also include an estimate of the experimental uncertainty in each of the measurements. The contributions to the overall uncertainty arise from counting statistics, the uncertainty in the helium standard cross section and uncertainties in the application of the relative flow technique (pressure, current and flow rate measurements). With the exception of the measurements at very low energies, and at minima in the DCS where statistical uncertainties are appreciable, the overall uncertainty in the absolute magnitude is generally around 10%. Phase shifts, derived from the phase-shift analysis of the present data at energies below 5 eV, are given in table 2 where they are compared with the present theoretical calculation and the phase shifts which arise from the calculation of Johnson and Guet (1994).

The lowest energy measurements in the present series, those at 0.67 eV, are shown in figure 1(*a*) where the DCS is also compared with that of Weyhreter *et al* (1988). Given the low incident energy and the substantial uncertainties in the present DCS, the level of agreement between the two cross sections, both in shape and absolute magnitude, is quite good. Whilst the present calculation is in good agreement with both experiments with regard to the shape of the DCS, and the absolute magnitude at forward angles, it lies below both sets of experimental data at larger scattering angles by 50–100%.

In figure 1(*b*) we illustrate the present measurements and calculations for an energy of 0.85 eV. Once again the agreement with the data of Weyhreter *et al* (1988) is quite good although the present DCS is slightly larger (20–30%) in magnitude in the mid-angle region. Also the experimental data are once again in good agreement with the present calculation at forward scattering angles but the experiment is about 50% larger at scattering angles of 90° and above. We also show the DCS resulting from a five-parameter phase-shift analysis (s-, $p_{1/2,3/2}$-, d- and f-waves) of the experimental DCS, which illustrates the level of agreement obtained with the fit. At an energy of 1.0 eV (figure 1(*c*)) we compare the present experimenta data with the measurements of Weyhreter *et al* (1988) and with the lowest energy measurement of Register *et al* (1986). In general, the level of agreement is very good although the present measurements indicate a deeper first minima which occurs at a slightly smaller scattering angle than in both of the other DCS. Otherwise the three cross sections generally agree to within the combined uncertainties at most angles. We also show the results of the present calculation, the calculation of Johnson and Guet (1994) and the calculation of McEachran and Stauffer (1987). The essential difference between the calculation of McEachran and Stauffer (1987) and the present is that the present includes the effects of dynamic distortion. There is a small, but significant, difference between these calculations at angles less than about 90°, the present calculation being in better agreement with experiment in terms of shape and absolute magnitude. This is typical of the differences

Table 1. Absolute differential cross sections (in units of 10^{-16} cm^2 sr^{-1}) for elastic electron scattering from xenon. Figures in parentheses indicate estimated percentage uncertainties and integral cross sections (σ_i and σ_m) are given in units of 10^{-16} cm^2. The estimated uncertainty on the integral cross sections is ±20%.

Angle	Energy (eV)					
(deg)	0.67	0.75	0.85	1.0	1.75	2.0
15				1.121(70)	0.712(7)	
20			0.876(77)	0.482(27)	0.375(7)	0.490(8)
25	1.11(49)	0.405(20)	0.398(21)	0.289(24)	0.168(9)	0.245(7)
27.5					0.108(7)	0.198(7)
30	0.456(19)	0.290(17)	0.234(12)	0.128(14)	0.0847(7)	0.149(7)
32.5				0.074 5(15)	0.086(7)	0.148(7)
35		0.154(10)	0.099 8(8)	0.040 6(18)	0.106(9)	0.170(8)
37.5			0.071 0	0.016 8(28)		
40	0.114(28)	0.076 2(12)	0.040 4(15)	0.010 2(23)	0.200(7)	0.277(7)
42.5			0.021 7(18)	0.005 98(46)		
45		0.028 2(32)	0.012 4(44)	0.012 6(25)	0.338(7)	0.425(7)
47.5		0.020 2(34)	0.008 25(49)			
50	0.0485(40)	0.004 98(141)	0.010 2(37)	0.035 9(11)	0.502(7)	0.622(7)
52.5						
55		0.012 5(65)	0.018 5(22)	0.077 2(10)	0.657(7)	0.815(7)
57.5		0.017 7(58)				
60	0.0261(51)	0.022 5(40)	0.047 4(8)	0.125(8)	0.814(7)	0.991(7)
65			0.077 1(8)	0.175(9)	0.935(7)	1.142(7)
70		0.049 7(13)	0.102(7)	0.208(9)	1.009(7)	1.221(7)
75			0.126(7)	0.238(9)	1.041(7)	1.278(7)
80	0.0451(37)	0.077 4(16)	0.139(7)	0.254(8)	1.027(7)	1.257(7)
85			0.142(7)	0.255(9)	0.967(7)	1.200(7)
90	0.0407(48)	0.087 0(13)	0.143(7)	0.254(8)	0.868(7)	1.057(7)
95			0.130(9)	0.234(9)	0.735(7)	0.925(7)
100	0.0500(43)	0.075 1(11)	0.111(8)	0.197(13)	0.603(7)	0.731(7)
105			0.096 5(7)	0.159(10)	0.451(7)	0.562(7)
110	0.0393(63)	0.051 1(17)	0.075 9(8)	0.124(10)	0.318(7)	0.384(7)
115			0.054 4(10)	0.072 3(14)	0.194(7)	0.238(7)
120	0.0325(96)	0.021 8(32)	0.035 9(25)	0.051 5(26)	0.0985(7)	0.117(7)
122.5					0.0660(7)	0.0801(8)
125			0.019 6(18)	0.027 0(29)	0.0404(8)	0.0479(8)
127.5			0.018 0(31)		0.0254(10)	0.0318(8)
130		0.017 2(100)	0.010 5(85)	0.017 7(41)	0.0206(13)	0.0275(12)
132.5			0.009 07(73)		0.0244(15)	0.0325(12)
135					0.0307(11)	0.0471(10)
σ_i	1.45	1.24	1.46	1.95	6.62	8.80
σ_m	0.41	0.51	0.74	1.32	5.69	8.21

Angle	Energy (eV)				
(deg)	2.75	3.75	5.0	7.9	10
15	1.874(8)	4.296(9)	10.358(8)	23.263(8)	21.068(7)
20	1.295(7)	3.132(7)	8.161(7)	15.063(7)	17.197(7)
25	0.864(7)	2.400(8)	6.232(7)	13.316(7)	13.406(7)
27.5					
30	0.612(7)	1.803(9)	4.796(7)	9.182(7)	10.139(7)
32.5	0.574(7)				
35	0.565(7)	1.497(7)	3.709(7)	7.481(7)	7.874(7)

Table 1. (Continued)

Angle (deg)	Energy (eV)				
	2.75	3.75	5.0	7.9	10
37.5	0.595(7)	1.392(7)			
40	0.658(7)	1.410(7)	2.993(7)	5.273(7)	5.719(8)
42.5		1.406(7)			
45	0.845(7)	1.477(7)	2.557(7)	4.010(7)	3.872(8)
47.5					
50	1.086(7)	1.677(7)	2.342(7)	2.990(8)	2.769(8)
52.5			2.272(7)		
55	1.366(7)	1.886(7)	2.316(7)	2.222(7)	2.063(7)
57.5			2.323(7)		
60	1.643(7)	2.253(8)	2.391(7)	1.789(7)	1.449(7)
65	1.867(7)	2.426(7)	2.531(7)	1.523(7)	1.127(8)
70	1.967(7)	2.583(7)	2.648(7)	1.389(7)	0.920(7)
75	2.044(7)	2.626(7)	2.671(7)	1.341(7)	0.787(7)
80	1.998(7)	2.510(7)	2.608(7)	1.298(7)	0.711(7)
85	1.891(7)	2.319(7)	2.439(7)	1.235(7)	0.672(8)
90	1.640(7)	2.045(7)	2.131(7)	1.143(7)	0.605(7)
95	1.368(7)	1.659(7)	1.721(7)	0.957(7)	0.549(7)
100	1.098(7)	1.258(7)	1.283(7)	0.830(7)	0.502(7)
105	0.781(7)	0.859(7)	0.835(7)	0.584(7)	0.450(9)
110	0.506(7)	0.467(10)	0.441(7)	0.456(7)	0.418(8)
115	0.261(7)	0.196(10)	0.142(7)	0.280(7)	0.413(8)
117.5			0.0621(8)		
120	0.112(8)	0.0497(14)	0.0239(7)	0.278(7)	0.435(7)
122.5	0.0631(7)	0.0347(12)	0.0347(7)		
125	0.0426(8)	0.0570(15)	0.0999(7)	0.369(7)	0.525(8)
127.5	0.0467(10)				
130	0.0732(9)	0.226(12)	0.385(7)	0.593(7)	0.655(7)
132.5					
σ_i	15.3	22.9	33.6	42.2	
σ_m	14.2	20.7	28.8	30.9	

Angle (deg)	Energy 20 eV	Angle (deg)	Energy (eV)		
			25	40	50
14	31.09(8)	10	38.26(12)	14.03(9)	11.72(12)
19	20.88(8)	15	23.51(14)	7.57(8)	4.77(7)
24	14.60(7)	20	13.69(15)	3.67(7)	1.94(7)
29	8.77(8)	25	9.42(9)	1.83(7)	0.699(7)
34	4.98(7)	30	5.01(11)	0.869(8)	0.238(8)
39	2.26(7)	35	2.54(8)	0.405(7)	0.085(8)
44	0.879(7)	40	0.948(12)	0.172(7)	0.030(8)
49	0.242(8)	45	0.223(14)	0.066(7)	0.0088(8)
51.5	0.154(8)	47.5	0.079(13)	0.045(8)	0.0037(11)
54	0.149(8)	50	0.074(10)	0.040(8)	0.0020(23)
56.5	0.226(7)	52.5	0.152(10)	0.046(8)	0.0032(17)
59	0.316(8)	55	0.258(8)	0.058(7)	0.0074(9)
64	0.525(7)	57.5	—	—	0.013(9)
69	0.691(8)	60	0.532(8)	0.092(8)	0.020(9)
74	0.720(8)	65	0.745(7)	0.120(8)	0.034(7)
79	0.631(7)	70	0.848(8)	0.127(7)	0.043(8)
84	0.455(8)	75	0.784(8)	0.119(8)	0.039(7)

Table 1. (Continued)

Angle (deg)	Energy 20 eV	Angle (deg)	Energy (eV) 25	40	50
89	0.278(8)	80	0.583(8)	0.099(8)	0.032(8)
94	0.143(9)	82.5	—	0.090(7)	—
96.5	0.093(9)	85	0.362(8)	0.085(8)	0.029(9)
99	0.067(10)	87.5	—	0.090(8)	0.036(12)
101.5	0.059(9)	90	0.173(8)	0.097(8)	0.048(8)
104	0.063(8)	92.5	0.088(9)	—	0.066(7)
106.5	0.081(9)	95	0.065(8)	0.146(8)	0.095(7)
109	0.113(8)	97.5	0.045(11)	—	0.131(7)
114	0.193(8)	100	0.056(8)	0.223(8)	0.173(9)
119	0.257(10)	102.5	0.066(8)	—	—
124	0.261(8)	105	0.120(9)	0.299(9)	0.269(9)
129	0.226(8)	110	0.210(7)	0.400(9)	0.377(9)
		115	0.273(7)	0.458(10)	0.449(10)
		120	0.277(7)	0.457(10)	0.464(11)
		125	0.209(9)	0.391(10)	0.423(10)
		130	0.100(10)	0.278(9)	0.311(10)

observed at most low energies resulting from the inclusion of dynamic distortion effects. All three calculations exhibit the same general cross section shape as the experiments and display good agreement in terms of the absolute magnitude of the main features of the cross section, although there are differences in the position of the first minima between each calculation and the present experiment. The calculation of Johnson and Guet (1994) also predicts the position of the mid-angle cross section maximum at an angle which is about 15° smaller than that observed in the experiment. In figure 1(*d*) we compare the present DCS with that of Weyhreter *et al* (1988) and Register *et al* (1986) at an energy of 1.75 eV and, once again, the agreement is extremely good, as is the accord between these experiments and the present calculation.

At 2.75 eV (figure 2(*a*)) we note some, relatively minor, discrepancies between the present experiment and that of Register *et al* (1986). The present experimental DCS is about 25% smaller in the region of the first minima and this minimum occurs at a slightly lower scattering angle in the present DCS than in that of Register *et al* (1986). Otherwise the two cross sections are in excellent agreement. The present calculation appears to be in slightly better agreement with the DCS of Register *et al* (1986). Once again we show the result of the phase-shift analysis fit, with six variable parameters, to the experimental DCS at this energy. At 3.75 eV (figure 2(*b*)) the discrepancy between the present data and that of Register *et al* (1986) at forward scattering angles persists, although at angles larger than 50° the level of agreement is excellent. The present calculation and, in particular that of Johnson and Guet (1994), are both in better agreement with the Register *et al* (1986) cross section at forward angles and both are in good agreement with experiment at large scattering angles.

At an energy of 5 eV (figure 2(*c*)), the present experiment is in excellent agreement with those of Register *et al* (1986) and Nishimura *et al* (1987) across the entire angular range. There are, however, big differences between these three measurements and those of Klewer *et al* (1980). The agreement with the calculation of Johnson and Guet (1994) and with the present calculation is generally good, although the former seems to provide a better

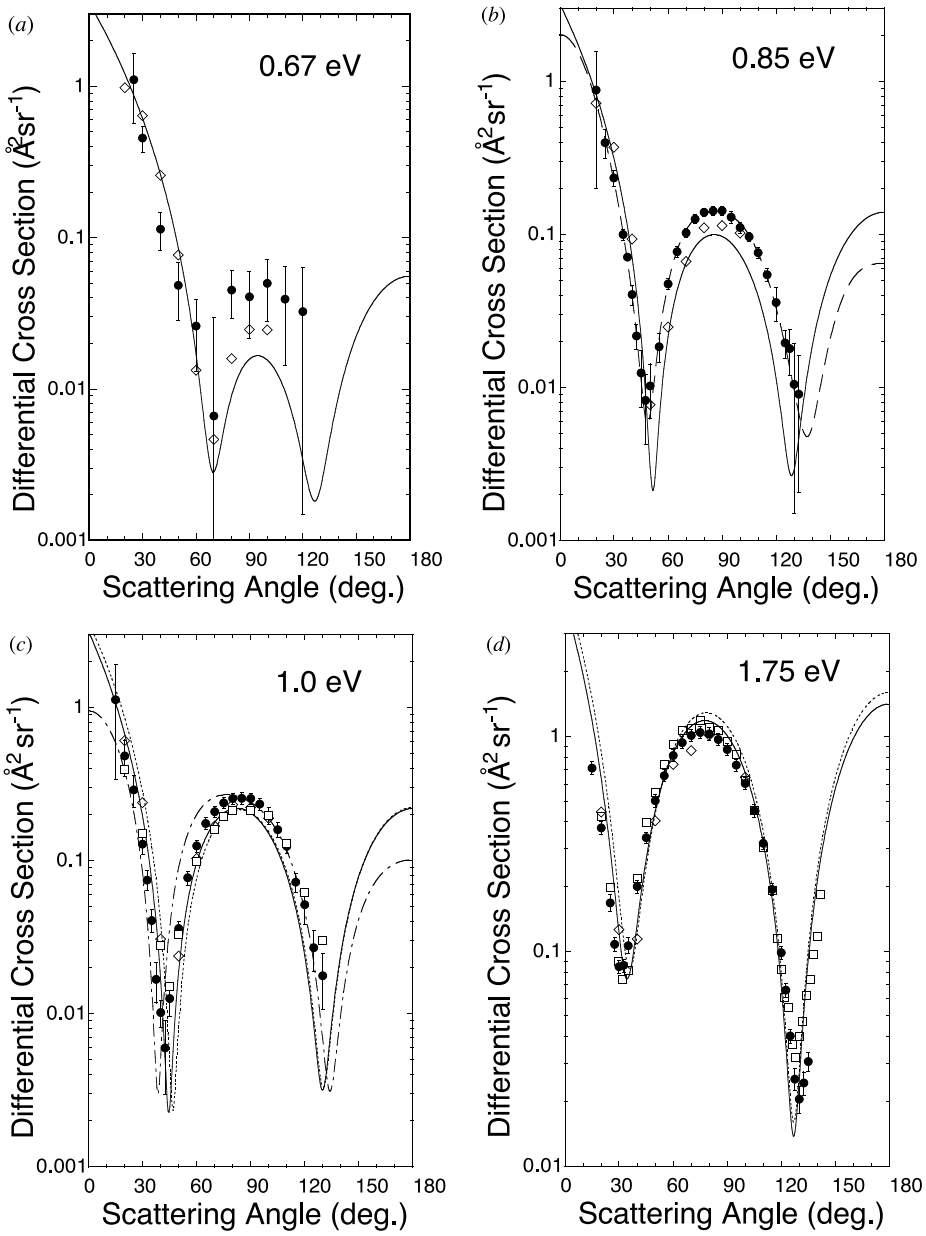

Figure 1. (*a*) Differential cross sections for elastic electron scattering from xenon at 0.67 eV. (●) Present experimental result, (◊) Weyhreter *et al* (1988), (——) present relativistic calculation. (*b*) Differential cross section for elastic electron scattering from xenon at 0.85 eV. (●) Present experimental result, (◊) Weyhreter *et al* (1988), (——) present relativistic calculation, (– – –) DCS derived from the phase-shift analysis of the present experimental data. (*c*) Differential cross section for elastic electron scattering from xenon at 1.0 eV. (●) Present experimental result, (◊) Weyhreter *et al* (1988), (□) Register *et al* (1986), (——) present relativistic calculation, (— · —) Johnson and Guet (1994), (· · · · · ·) McEachran and Stauffer (1987). (*d*) Differential cross section for elastic electron scattering from xenon at 1.75 eV. (●) Present experimental result, (◊) Weyhreter *et al* (1988), (□) Register *et al* (1986), (——) present relativistic calculation, (· · · · · ·) McEachran and Stauffer (1987).

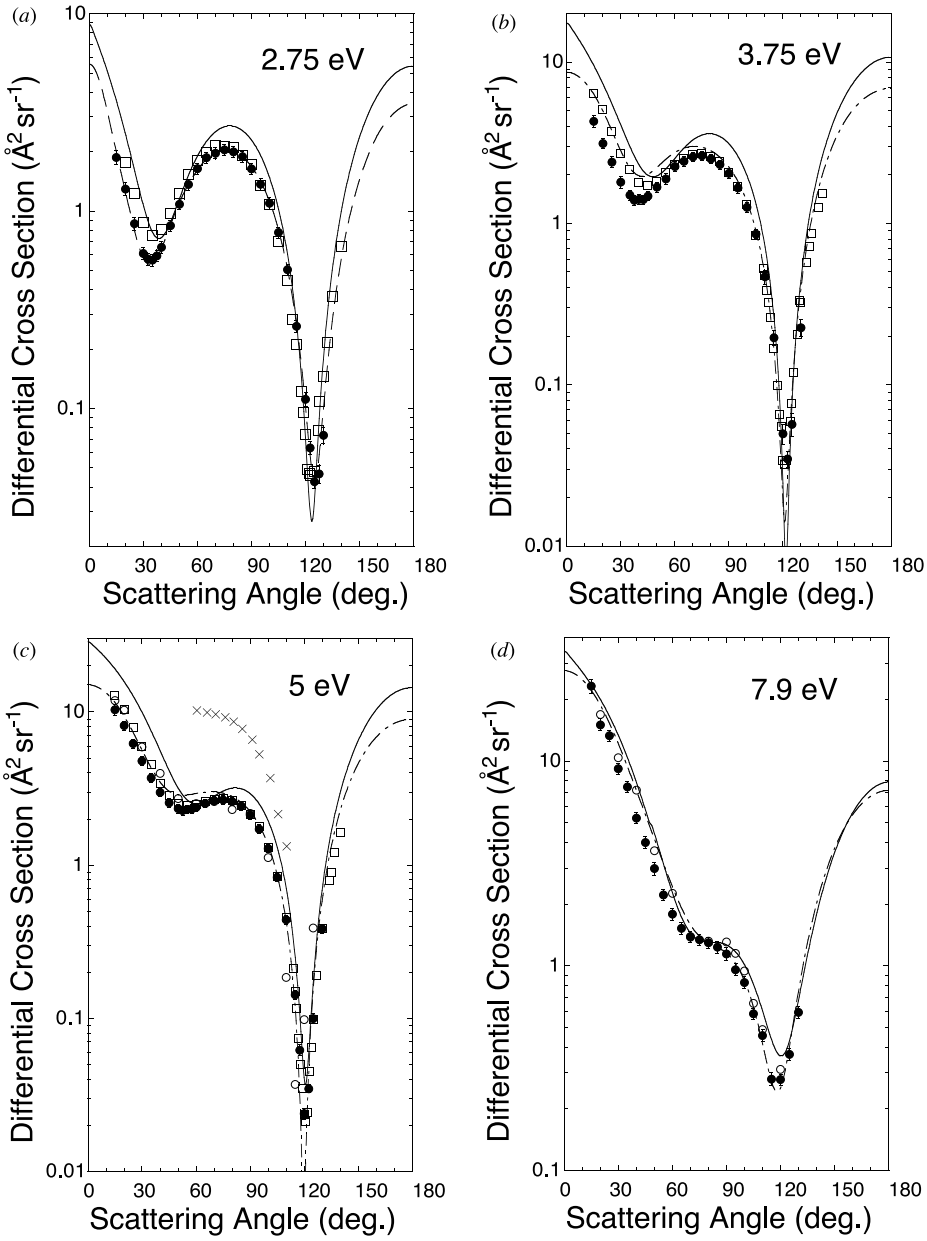

Figure 2. (*a*) Differential cross section for elastic electron scattering from xenon at 2.75 eV. (●) Present experimental result, (□) Register *et al* (1986), (——) present relativistic calculation, (– – –) DCS derived from the phase-shift analysis of the present experimental data. (*b*) Differential cross section for elastic electron scattering from xenon at 3.75 eV. (●) Present experimental result, (□) Register *et al* (1986), (——) present relativistic calculation, (— · —) Johnson and Guet (1994). (*c*) Differential cross section for elastic electron scattering from xenon at 5 eV. (●) Present experimental result, (×) Klewer *et al* (1980), (□) Register *et al* (1986), (○) Nishimura *et al* (1987), (——) present relativistic calculation, (— · —) Johnson and Guet (1994). (*d*) Differential cross section for elastic electron scattering from xenon at 7.9 eV. (●) Present experimental result, (○) Nishimura *et al* (1987) at 8 eV, (——) present relativistic calculation, (— · —) Johnson and Guet (1994) at 8 eV.

Table 2. Elastic electron scattering phase shifts for xenon (in radians).

Energy (eV)	Partial wave	Present experiment	Present theory	Johnson and Guet (1994)
0.67	$s_{1/2}$	0.059 07	0.060 73	
	$p_{1/2}$	0.067 58	0.053 23	
	$p_{3/2}$	−0.007 307	0.030 05	
	$d_{3/2}$	0.061 22	0.047 23	
	$d_{5/2}$	—	0.047 77	
0.75	$s_{1/2}$	−0.000 005	0.032 3	
	$p_{1/2}$	0.057 5	0.048 9	
	$p_{3/2}$	0.008 177	0.022 9	
	$d_{3/2}$	0.055 8	0.054 4	
	$d_{5/2}$	—	0.055 1	
0.85	$s_{1/2}$	−0.040 53	−0.002 0	
	$p_{1/2}$	0.063 83	0.042 3	
	$p_{3/2}$	0.010 77	0.012 9	
	$d_{3/2}$	0.057 1	0.063 9	
	$d_{5/2}$	—	0.064 8	
1.0	$s_{1/2}$	−0.080 86	−0.051 3	−0.101 5
	$p_{1/2}$	0.047 9	0.030 0	0.016 75
	$p_{3/2}$	−0.010 41	−0.004 0	−0.014 57
	$d_{3/2}$	0.075 4	0.079 5	0.070 36
	$d_{5/2}$	—	0.080 8	0.071 29
1.75	$s_{1/2}$	−0.294 1	−0.264 4	
	$p_{1/2}$	−0.024 97	−0.051 27	
	$p_{3/2}$	−0.104 87	−0.103 8	
	$d_{3/2}$	0.157 7	0.184 1	
	$d_{5/2}$	—	0.189 0	
2.0	$s_{1/2}$	−0.344 2	−0.326 2	−0.343 8
	$p_{1/2}$	−0.073 76	−0.081 5	−0.093 95
	$p_{3/2}$	−0.123 9	−0.138 8	−0.148 6
	$d_{3/2}$	0.198 8	0.230 2	0.183 9
	$d_{5/2}$	—	0.236 7	0.187 9
2.75	$s_{1/2}$	−0.486 7	−0.491 6	
	$p_{1/2}$	−0.141 1	−0.173 1	
	$p_{3/2}$	−0.229 7	−0.241 7	
	$d_{3/2}$	0.325 4	0.402 6	
	$d_{5/2}$	—	0.414 0	
3.75	$s_{1/2}$	−0.557 5	−0.678 8	
	$p_{1/2}$	−0.209 8	−0.290 6	
	$p_{3/2}$	−0.422 2	−0.369 4	
	$d_{3/2}$	0.487 1	0.686 7	
	$d_{5/2}$	—	0.699 8	

description of the shape of the DCS at forward angles. The final example of the elastic DCS at an energy below the first inelastic threshold is shown in figure 2(*d*) at an energy of 7.9 eV. This energy corresponds to that of the $5p^5(^2P_{3/2})6s^2\,^1S$ negative ion resonance (see e.g. Buckman and Clark 1994). The present DCS is once again in good agreement with that of Nishimura *et al* (1987) and with both the present calculation and that of Johnson and Guet (1994). Note that the DCS of Nishimura *et al* (1987) and Johnson and Guet (1994) are for an energy of 8 eV.

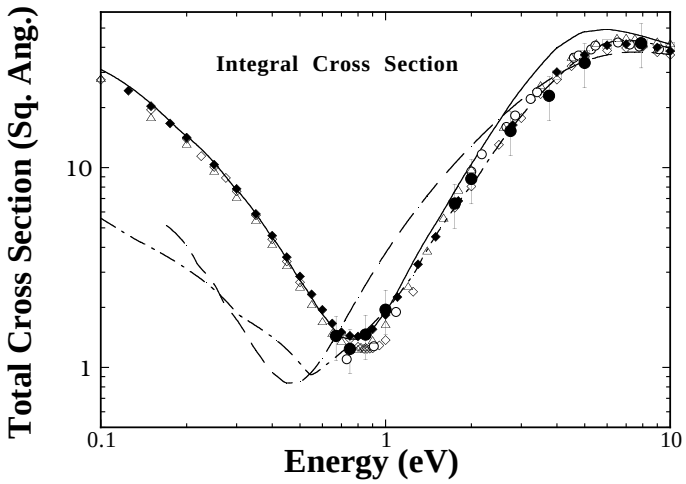

Figure 3. Integral elastic scattering cross section for xenon between 0.1 and 10 eV. (●) Present experimental result, (□) Nickel *et al* (1985), (⧫) Ferch *et al* (1987), (△) Jost *et al* (1983), (○) Subramanian and Kumar (1987), (◊) Alle *et al* (1993), (——) present relativistic calculation, (— · —) Johnson and Guet (1994), (— — —) Gianturco and Rodriguez-Ruiz (1994).

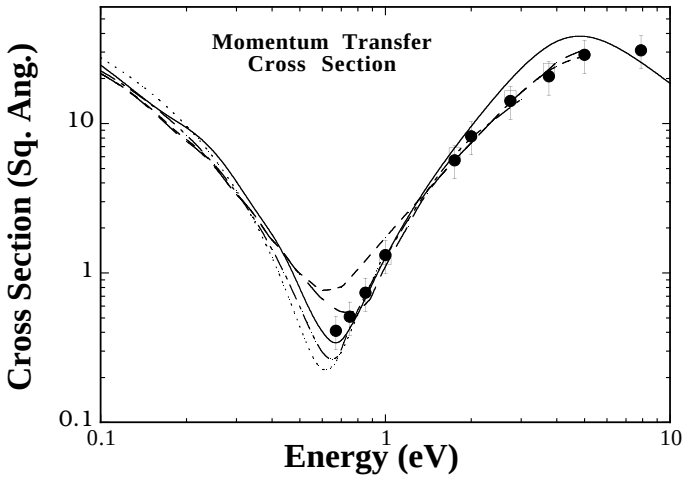

Figure 4. Elastic momentum transfer cross section for xenon between 0.1 and 10 eV. (●) Present experimental result, (□) Register *et al* (1986), (· · · · · ·) Weyhreter *et al* (1988), (- - - -) Hunter *et al* (1988), (– – –) Nakamura (1991), (— · —) Schmidt *et al* (1994), (——) present relativistic calculation.

5.2. Integral cross sections

Integral elastic and elastic momentum transfer cross sections have been derived from the present DCS measurements via the phase-shift analysis technique. These cross sections are given in table 2 and presented graphically in figures 3 and 4. There is a substantial body of work with which they can be compared and, in the interests of clarity, we have chosen to make the comparisons with only a selection of these previous measurements. For the integral elastic cross section (figure 3) the present measurements extend to low

enough energies to show the deep R–T minimum which occurs at around 0.8 eV. Within the combined uncertainties of the present data and previous measurements, the level of agreement between the various experiments is reasonably good, with the best level of agreement being demonstrated with the cross sections of Ferch *et al* (1987), Jost *et al* (1983) and Alle *et al* (1993). For energies less than 2 eV the present calculation is also in excellent agreement with these various experiments. Above 2 eV, the calculated cross section is slightly higher than the experiments, reflecting the differences observed, and commented upon above, in the differential cross sections.

In figure 4 we show the momentum transfer cross section and once again the present experiment and theory are in good agreement with each other and with the derived cross section of Register *et al* (1986) for energies less than 2 eV. Above this energy the present experiment and that of Register *et al* (1986) remain in good agreement although both are smaller in magnitude than the present calculation. At lower energies it would appear that the present measurements favour a lower R–T minimum in σ_m than is predicted by either of the swarm-derived cross sections of Hunter *et al* (1988) or Nakamura (1991). This brings it into better agreement with the swarm-derived cross section of Schmidt *et al* (1994) and with the cross section of Weyhreter *et al* (1988) which was derived from crossed-beam measurements via the use of modified effective range theory. The present measurements and theory are in excellent agreement below 2 eV.

6. Conclusions

We have presented a comprehensive set of differential cross section measurements and calculations for elastic scattering of electrons from Xe at energies between 0.67 and 50 eV. The experimental measurements provide only the second set of such absolute data at energies below 1 eV. In general the agreement with previous experiments is encouraging, although there are some instances where the comparison reveals discrepancies which are outside of the combined experimental uncertainties. These differences are larger and arise somewhat more frequently than those which we have observed previously in comparisons of cross sections for Ne (Gulley *et al* 1994) and Ar (Gibson *et al* 1996). No doubt this is due in some part to the more stringent requirements on angular resolution that are imposed by the detailed structure in the low-energy electron–xenon cross section.

The level of agreement with theory is also encouraging. In the case of the present relativistic calculation this agreement is best at energies below 8 eV. At energies above this the calculation provides an excellent description of the shape of the DCS but there are some differences in the absolute magnitude. These may be due, in part, to the fact that the present calculation does not account for the loss of flux from the elastic channel as a result of inelastic scattering (absorption effects). We also note a good level of agreement with the recent relativistic, many-body perturbation theory calculation of Johnson and Guet (1994) at energies of 1–8 eV.

The experimental data have been analysed using a ‘relativistic’ phase-shift technique which has enabled us to extract s-, $p_{1/2,3/2}$-, and d-wave phase shifts for comparison with theory. These phase shifts can, in turn, be further used to calculate Sherman functions for comparison with experiment (Buckman *et al* 1997).

Acknowledgments

It is a pleasure to acknowledge the expertise of the technical staff of the Electron Physics Group without whom these measurements would not have been possible. We also thank Professor W Johnson and Professor F Hanne for the provison of tabulated data. JCG gratefully acknowledges the ANU Graduate School for the provision of a Research Scholarship and DRL gratefully acknowledges the Australian Research Council for the award of a Postdoctoral Fellowship. RPM acknowledges the support of the Natural Sciences and Engineering Research Council of Canada.

References

Ali M K and Fraser P A 1977 *J. Phys. B: At. Mol. Phys.* **10** 3091
Alle D T, Brennan M J and Buckman S J 1993 *XVIII Int. Conf. on Physics of Electronic and Atomic Collisions (Aarhus)* p 127
Alle D T, Gulley R J, Buckman S J and Brunger M J 1992 *J. Phys. B: At. Mol. Opt. Phys.* **25** 1533
Allen L J 1986 *Phys. Rev.* A **34** 2706
Brunger M J, Buckman S J, Allen L J, McCarthy I E and Ratnavelu K 1992 *J. Phys. B: At. Mol. Opt. Phys.* **25** 1823
Buckman S J and Clark C W 1994 *Rev. Mod. Phys.* **66** 539
Buckman S J, Gulley R J, Moghbelalhossein M and Bennett S J 1993 *Meas. Sci. Technol.* **4** 1143
Buckman S J, Lun D R, Gibson J C, Allen L J, McEachran R P and Parcell L A 1997 *J. Phys. B: At. Mol. Opt. Phys.* **30** L619
Callaway J, LaBahn R W, Pu R T and Duxler W M 1968 *Phys. Rev.* **168** 12
Ferch J, Simon F and Strakeljahn G 1987 *XV Int. Conf. on Physics of Electronic and Atomic Collisions (New York)* p 132
Gianturco F A and Rodriguez-Ruiz J A 1994 *Z. Phys.* D **31** 149
Gibson J C, Gulley R J, Sullivan J P, Buckman S J, Chan V and Burrow P D 1996 *J. Phys. B: At. Mol. Opt. Phys.* **29** 3177
Grant I P, McKenzie B J, Norrington P H, Mayers D F and Pyper N C 1980 *Comput. Phys. Commun.* **21** 207
Gulley R J, Alle D T, Brennan M J, Brunger M J and Buckman S J 1994 *J. Phys. B: At. Mol. Opt. Phys.* **27** 2593
Gulley R J, Brunger M J and Buckman S J 1993 *J. Phys. B: At. Mol. Opt. Phys.* **26** 2913
Hunter S, Carter J G and Christophorou L G 1988 *Phys. Rev.* A **38** 58
Johnson W R and Guet C 1994 *Phys. Rev.* A **49** 1041
Jost K, Bisling P G F, Eschen F, Felsmann M and Walther L 1983 *XII Int. Conf. on the Physics of Electronic and Atomic Collisions (Berlin)* (Berlin: ICPEAC) p 91
Kessler J 1985 *Polarised Electrons* 2nd edn (Berlin: Springer).
——1991 *Adv. At. Mol. Opt. Phys.* **27** 81
Klewer M, Beerlage M J M and van der Wiel M J 1980 *J. Phys. B: At. Mol. Opt. Phys.* **13** 571
LaBahn R W and Callaway J 1966 *Phys. Rev.* **147** 28
McEachran R P and Stauffer A D 1983a *J. Phys. B: At. Mol. Opt. Phys.* **16** 255
——1983b *J. Phys. B: At. Mol. Opt. Phys.* **16** 4023
——1984 *J. Phys. B: At. Mol. Opt. Phys.* **17** 2507
——1987 *J. Phys. B: At. Mol. Opt. Phys.* **20** 3483
——1988 *Proc. Int. Symp. on Correlation and Polarisation in Electronic and Atomic Collisions* (Singapore: World Scientific) p 183
——1990 *J. Phys. B: At. Mol. Opt. Phys.* **23** 4605
——1997 *Aust. J. Phys.* **50** 511–24
Mimnagh D J R, McEachran R P and Stauffer A D 1993 *J. Phys. B: At. Mol. Opt. Phys.* **26** 1727
Nakamura Y 1991 *Joint Symp. on Electron and Ion Swarms and Low Energy Electron Scattering (Brisbane)* Abstracts p 103
Nesbet R K 1979 *Phys. Rev.* A **20** 58
Nickel J C, Imre K, Register D F and Trajmar S 1985 *J. Phys. B: At. Mol. Phys.* **18** 125
Nishimura H, Matsuda T and Danjo A 1987 *J. Phys. Soc. Japan* **56** 70
Petrovic Z L, O'Malley T F and Crompton R W 1995 *J. Phys. B: At. Mol. Opt. Phys.* **28** 3309
Register D F, Vuskovic L and Trajmar S 1986 *J. Phys. B: At. Mol. Opt. Phys.* **19** 1685

Rohr K 1977 *J. Phys. B: At. Mol. Phys.* **10** 2215
Schmidt B, Berkhan K, Götz B and Müller M 1994 *Phys. Scr.* **53** 30
Subramanian K P and Kumar V 1987 *J. Phys. B: At. Mol. Opt. Phys.* **20** 5505
Temkin A 1957 *Phys. Rev.* **107** 1004
Temkin A and Lamkin J C 1961 *Phys. Rev.* **121** 788
Weyhreter M, Barzick B, Mann A and Linder F 1988 *Z. Phys.* D **7** 333
Yuan J 1995 *Z. Phys.* D **35** 3